



**HAL**  
open science

## Field-effect passivation of Si by ALD-Al<sub>2</sub>O<sub>3</sub>: second harmonic generation monitoring and simulation

D Damianos, G. Vitrant, A. Kaminski-Cachopo, D. Blanc-Pélissier, G. Ghibaudo, M Lei, J Changala, A. Bouchard, X. Mescot, M Gri, et al.

### ► To cite this version:

D Damianos, G. Vitrant, A. Kaminski-Cachopo, D. Blanc-Pélissier, G. Ghibaudo, et al.. Field-effect passivation of Si by ALD-Al<sub>2</sub>O<sub>3</sub>: second harmonic generation monitoring and simulation. *Journal of Applied Physics*, 2018, 124 (12), pp.125309. 10.1063/1.5041062 . hal-01883529

**HAL Id: hal-01883529**

**<https://hal.science/hal-01883529>**

Submitted on 28 Sep 2018

**HAL** is a multi-disciplinary open access archive for the deposit and dissemination of scientific research documents, whether they are published or not. The documents may come from teaching and research institutions in France or abroad, or from public or private research centers.

L'archive ouverte pluridisciplinaire **HAL**, est destinée au dépôt et à la diffusion de documents scientifiques de niveau recherche, publiés ou non, émanant des établissements d'enseignement et de recherche français ou étrangers, des laboratoires publics ou privés.

FIELD-EFFECT PASSIVATION OF SI BY ALD- $\text{Al}_2\text{O}_3$ :  
SECOND HARMONIC GENERATION MONITORING AND SIMULATION

D. Damianos<sup>\*(1)</sup>, G. Vitrant<sup>(1)</sup>, A. Kaminski-Cachopo<sup>(1)</sup>, D. Blanc-Pelissier<sup>(2)</sup>, G. Ghibaudo<sup>(2)</sup>,  
M. Lei<sup>(3)</sup>, J. Changala<sup>(3)</sup>, A. Bouchard<sup>(1)</sup>, X. Mescot<sup>(1)</sup>, M. Gri<sup>(1)</sup>, S. Cristoloveanu<sup>(1)</sup>, I. Ionica<sup>(1)</sup>

<sup>(1)</sup>Univ. Grenoble Alpes, CNRS, Grenoble-INP\*\*, IMEP-LAHC, 38000 Grenoble, France

<sup>(2)</sup>INL - UMR 5270, INSA de Lyon, 7 avenue Jean Capelle, 69621 Villeurbanne, France

<sup>(3)</sup>FemtoMetrix, 1850 East Saint Andrew Place, Santa Ana, CA 92705, USA

\*Corresponding author: [dimitrios.damianos@minatec.grenoble-inp.fr](mailto:dimitrios.damianos@minatec.grenoble-inp.fr)

*Abstract* – This paper investigates the ability of second harmonic generation (SHG) to probe the passivation quality of atomic layer deposited (ALD)  $\text{Al}_2\text{O}_3$  on Si by estimating the induced interface electric field due to fixed charges in the oxide. Samples with various oxide charges ( $Q_{\text{ox}}$ ) and interface state densities ( $D_{\text{it}}$ ) were fabricated, using different deposition parameters. The samples were characterized by capacitance-voltage (C-V) and microwave photoconductance decay ( $\mu$ -PCD) measurements in order to evaluate  $Q_{\text{ox}}$  and  $D_{\text{it}}$ , as well as the effective minority carrier lifetime  $\tau_{\text{eff}}$ . The SHG results were consistent with  $Q_{\text{ox}}$ ,  $D_{\text{it}}$  and  $\tau_{\text{eff}}$  values, proving the ability of the technique to monitor the interfacial quality in a contactless and non-destructive way. Optical simulations which use the electric field values obtained from the C-V measurements could reproduce the measured SHG signal. This demonstrates that SHG coupled with optical simulation can give access to the electric field magnitude and thus characterize the electrical properties of oxide/Si interfaces.

*Keywords* – Second Harmonic Generation, non-destructive characterization, high-k,  $\text{Al}_2\text{O}_3$ , surface passivation, interface electric field.

## I. Introduction

The increase in device performance and yield for photovoltaics and microelectronics applications necessitates excellent interface quality between materials. For example in silicon, the concentration of electrically active interface defects like  $P_b$ -type centers [1], [2], can be decreased by depositing different dielectrics [3], [4] on its surface. Within this context,  $Al_2O_3$  is known to provide excellent surface passivation of crystalline silicon and is used for both photodetectors and solar cells [4].  $Al_2O_3$  is an interesting choice due to its combined capabilities of reducing  $P_b$  centers by chemical passivation and field-effect passivation by negative charges, and the ability to use nm thick films while achieving an excellent stability during different processing steps [4].

The challenge in achieving excellent surface/interface quality in the fabrication process also requires effective characterization techniques. The demand for contactless, non-destructive inspection of the interface quality in new substrates (Silicon-on-Insulator, III-V, etc...) and high-k dielectrics on Si is escalating, since conventional electrical measurement methods are mostly invasive [5] and/or entail specific device fabrication.

In order to monitor the efficiency of surface passivation, various contactless techniques are conventionally employed. For example, Microwave Photoconductance Decay ( $\mu$ -PCD) serves for minority carrier lifetime extraction [6]. However, a decorrelation between field-effect and chemical passivation is hardly possible with this technique. Additionally, for  $\mu$ -PCD measurements it is necessary to passivate both surfaces of the wafer in order to suppress predominant surface recombination when measuring the effective lifetime [4], [7].

Another contactless technique is corona oxide characterization of semiconductors (COCOS) [8] where charges are deposited through a corona discharge on the surface of the oxide-semiconductor stack, and are subsequently measured with a Kelvin probe [6]. These deposited charges compensate the field-effect passivation caused by the built-in charges at the oxide-semiconductor interface. COCOS allows the measurement of the fixed charge and interface trap densities, but after each measurement the surface of the sample under study needs to be wiped (for example with alcohol or de-ionized water [8]) in order to remove the deposited corona charges.

A very promising diagnostic can be second harmonic generation (SHG), a contactless and noninvasive, nonlinear optical technique which is complementary to  $\mu$ -PCD and COCOS, but does not require any prior- or post- treatment of the samples under study [9].

When using centrosymmetric materials (such as bulk Si and amorphous Al<sub>2</sub>O<sub>3</sub>), no 2<sup>nd</sup> order polarization is allowed in the dipolar approximation: SHG is therefore forbidden in the bulk of these materials [10]. Nevertheless, at the interface between two media the inversion symmetry is broken and a tensorial second order susceptibility is present. Symmetry breaking can also appear due to the static electric field that typically exists perpendicular to the interfaces of oxides and semiconductors. The SH intensity obtained in reflection [10] from a single interface is then given by the squared modulus of the second order polarization vector [11]:

$$I_{2\omega} \propto (P_{2\omega})^2 \propto \left| \overset{\leftrightarrow}{\chi}_{\text{interface}}^{(2)} + \overset{\leftrightarrow}{\chi}^{(3)} \overline{E}_0 \right|^2 I_{\omega}^2 \quad (1)$$

where  $\overset{\leftrightarrow}{\chi}_{\text{interface}}^{(2)}$  is the second order nonlinear susceptibility tensor arising from the symmetry breaking at the interface due to lattice mismatch between the two media;  $\overset{\leftrightarrow}{\chi}^{(3)} \overline{E}_0$  is the product of a third order bulk nonlinear susceptibility and the static electric field at the interface;  $I_{\omega}$  is the intensity of the incident optical field at the fundamental frequency. The term  $\overset{\leftrightarrow}{\chi}^{(3)} \overline{E}_0$  describes the Electric Field Induced Second Harmonic (EFISH) effect [9], [11] which has proven to be a very sensitive probe for internal electric fields [12]–[15]. The  $\overline{E}_0$  field is readily connected with the residual charges and with the interface trap density inside the oxide by Gauss' law. Under illumination, this field can vary in time since photo-generated electrons inside silicon can be injected into the oxide layer by multi-photon processes [13], [15], thus giving rise to a time dependent EFISH effect. Eq. 1 then becomes:

$$I_{2\omega} \propto \left| \overset{\leftrightarrow}{\chi}_{\text{interface}}^{(2)} + \overset{\leftrightarrow}{\chi}^{(3)} (\overline{E}_{dc} + \overline{E}(t)) \right|^2 (I_{\omega})^2 \quad (2)$$

where  $E_{dc}$  is the initial static dc electric field and  $E(t)$  is the time-dependent field related to trapping and detrapping phenomena of photo-induced carriers.

Previous studies have demonstrated the great capabilities of SHG characterization for dielectrics (SiO<sub>2</sub> and high-k) on Si, bringing remarkable insights into surface and buried interface studies. It has been reported [15], [16], that the trapping process for dielectrics on Si occurs via injection of electrons excited by the fundamental beam from the Si valence band into the oxide conduction band by 3-photon processes. For high-k dielectrics (Al<sub>2</sub>O<sub>3</sub>, ZrO<sub>2</sub> and HfO<sub>2</sub>) on Si, SHG has been applied to study the so-called ‘‘optical roughness’’, a quantity

that reflects the non-uniform distribution of the interfacial defects capable of charge trapping [16], as well as for monitoring the charge-trapping dynamics. In the same paper, detrapping was evidenced by a decrease of the SHG signal with time, and was significantly suppressed in high-k films, in contrast to SiO<sub>2</sub>, due to reduced leakage currents. Charge trapping defects in high-k stacks such as Si/SiO<sub>2</sub>/HfO<sub>2</sub>, have been characterized by spectroscopic SHG and time-dependent EFISH generation [17]: oxygen vacancy defects in HfO<sub>2</sub> films were identified and charge trapping in Hf-silicate samples was shown to be dominated by oxide surface defects. For the particular case of Al<sub>2</sub>O<sub>3</sub>, spectroscopic and time-dependent SHG revealed a fixed negative charge in thin Al<sub>2</sub>O<sub>3</sub> layers that increases after annealing (from 10<sup>11</sup> cm<sup>-2</sup> before anneal, up to 10<sup>12</sup>-10<sup>13</sup> cm<sup>-2</sup> after anneal) [18]. SHG was shown to be directly sensitive to the electric field in the SCR induced by these fixed negative charges and was used to distinguish between the influence of field-effect and chemical passivation. Both the amount of charges that can be injected into Al<sub>2</sub>O<sub>3</sub> and their net rates increased after annealing [18]. Spectroscopic SHG was also used to distinguish the impact of field-effect passivation and chemical passivation for different thicknesses (2-20 nm) of Al<sub>2</sub>O<sub>3</sub> on Si [19]. In the same work, they demonstrated that the field-effect passivation was virtually unaffected by the Al<sub>2</sub>O<sub>3</sub> thickness down to 2 nm for the plasma-assisted ALD and 5 nm for the thermal ALD process. Other studies [20], [21] including spectroscopic SHG, time-dependent SHG, and rotational angle SHG have shown that an interfacial SiO<sub>x</sub> layer (present between Al<sub>2</sub>O<sub>3</sub> and Si) and its thickness play an important role in the density and polarity of the interface charges. Another work [22] identified the differences between the passivation mechanisms of H<sub>2</sub>O-based and plasma-based ALD processes for Al<sub>2</sub>O<sub>3</sub> deposition: EFISH suggested significant differences in pre-existing charge density leading to different levels of field-effect passivation between the films deposited by the two ALD processes.

Even though in the literature the SHG method has been used for characterization of the electronic properties of Al<sub>2</sub>O<sub>3</sub> films on Si, it would be ideal to extract electrical information from a contactless SHG experiment, without extra processing steps. One of the difficulties arises from the fact that SHG signal contains both optical propagation phenomena (thickness dependent) and interface electric field (quality dependent). In order to use SHG as a stand-alone diagnostic tool for charge and interface state determination, a relationship between the SHG intensity and the built-in fixed charge density or interface trap density should be established. In our paper, C-V measurements were used to quantify the fixed

charge and trap densities (therefore the dc field) which were associated with SHG parameters and optical simulation.

In section II the sample fabrication is presented along with preliminary characterization by  $\mu$ -PCD and C-V. In section III the SHG results are shown. Firstly, time dependent SHG is performed on  $\text{Al}_2\text{O}_3/\text{Si}$  samples for initial comparison with the interface trap densities extracted from C-V measurements. Then, SHG is associated with minority carrier lifetime and fixed charge values obtained from  $\mu$ -PCD and C-V, accordingly. Finally, in section IV the need for optical simulation is expressed and a procedure to extract electrical information is proposed.

## **II. Sample preparation and preliminary characterization**

### **A. Sample fabrication**

Si wafers were double-side polished FZ p-type (0.8  $\Omega\text{cm}$  resistivity) with [100] surface orientation. The substrates were subsequently treated using a standard cleaning process to remove organic residuals and diluted HF to etch the native oxide. Thin  $\text{Al}_2\text{O}_3$  films (between 5 and 25 nm) were deposited at 250°C on both sides of the substrates using either thermal or plasma ALD in an Ultratech Fiji F200 reactor. Trimethylaluminium ( $\text{Al}(\text{CH}_3)_3$ ) was used as the reactant and water or oxygen were used as oxidants for the thermal and plasma process respectively. After deposition, the samples were cut in half: the 1<sup>st</sup> half was used as a reference and the 2<sup>nd</sup> half was subjected to a post-deposition anneal at 400°C for 10 min. The annealing step is known to reduce the interfacial trap density through hydrogen diffusion (chemical passivation) and to activate the negative charges close to the  $\text{Al}_2\text{O}_3/\text{Si}$  interface (field-effect passivation), which increases the lifetime [23]. The plasma ALD process has been reported to induce many defects leading to degradation of the interface of as-deposited samples due to the VUV radiation from the plasma [20], [22], [24]. However, after annealing, the large concentration of fixed charges combined with a good chemical passivation, lead to a very good quality of the  $\text{Al}_2\text{O}_3/\text{Si}$  interface [25].

## B. Lifetime characterization

For our SHG calibration needs, a panel of samples with different  $\text{Al}_2\text{O}_3$  film thicknesses and passivation quality was chosen. The surface passivation of each sample was probed by  $\mu$ -PCD measurements using a Semilab instrument [26]. Table I shows the average minority carrier lifetime ( $\tau_{\text{eff}}$ ) values of four samples, as-deposited (by plasma and thermal ALD) and annealed. The very low value of  $\tau_{\text{eff}}$  for the as-deposited plasma-ALD sample (P0) is expected due to a lack of hydrogen during the process (which consequently is responsible for high  $D_{\text{it}}$  values [3]). Annealing is known to reduce the interfacial trap density through hydrogen diffusion (chemical passivation) and to activate the negative charges close to the  $\text{Al}_2\text{O}_3/\text{Si}$  interface (field-effect passivation) [23], [27]. This reduces the surface recombination velocity, which in turn increases the lifetime as evidenced in Table 1. However, the lifetime for sample P1 is very low compared to values reported in the literature [3], [23], [27], [28]. This sample, which is not representative of annealed plasma ALD process, was specifically chosen for the SHG calibration due to its poor surface passivation, probably caused by contamination during the cleaning procedure.

Table I:  $\mu$ -PCD lifetime values for Si samples passivated with a 15 nm  $\text{Al}_2\text{O}_3$  film

Sample name	Process	Average minority carrier lifetime $\tau_{\text{eff}}$ ( $\mu\text{s}$ )
P0	Plasma ALD as deposited	3.5
P1	Plasma ALD annealed	65
T0	Thermal ALD as deposited	120
T1	Thermal ALD annealed	520

## C. C-V measurements for $D_{\text{it}}$ and $Q_{\text{ox}}$ extraction

We used the established conventional C-V technique in order to extract the fixed charges ( $Q_{\text{ox}}$ ) and interface traps ( $D_{\text{it}}$ ) that will be used later for SHG data analysis. Evaporation of approximately 200 nm thick Al through a shadow mask was necessary for the fabrication of circular MOS capacitors with 200  $\mu\text{m}$  diameter. C-V measurements were performed on all samples with a LCR meter in the parallel  $C_p$ - $G_p$  model [29]. The total capacitance  $C_m$  was measured as a function of the gate voltage  $V_G$ . The gate voltage was

swept from negative to positive values (accumulation to inversion) with a step of 100 mV. The delay time for the sweep was 1s in order to achieve equilibrium conditions for each measurement point. The ac signal level was set at 30 mV for frequencies ranging from 10kHz to 1 MHz.

$C_m$  was plotted versus  $V_G$  at 1 MHz, for the samples prepared by plasma ALD (Figure 1a for samples P0-P1) and thermal ALD (Figure 1b for samples T0-T1). In this figure we distinguish the three characteristic regions of the C-V curve [6], [29]:

- The accumulation region for negative  $V_G$ , where  $C_m$  is given by the oxide capacitance  $C_{ox}$  (maximum capacitance).
- The depletion region, where  $C_m$  starts to drop due to the silicon capacitance  $C_{Si}$  which is connected in series with  $C_{ox}$  ( $C_m^{-1} = C_{ox}^{-1} + C_{Si}^{-1}$ ). The value of  $V_G$  at which the accumulation region changes to depletion is the flat band voltage  $V_{FB}$ .
- The inversion region for positive  $V_G$ , where  $C_m$  saturates since the depletion width in Si reaches its maximum.

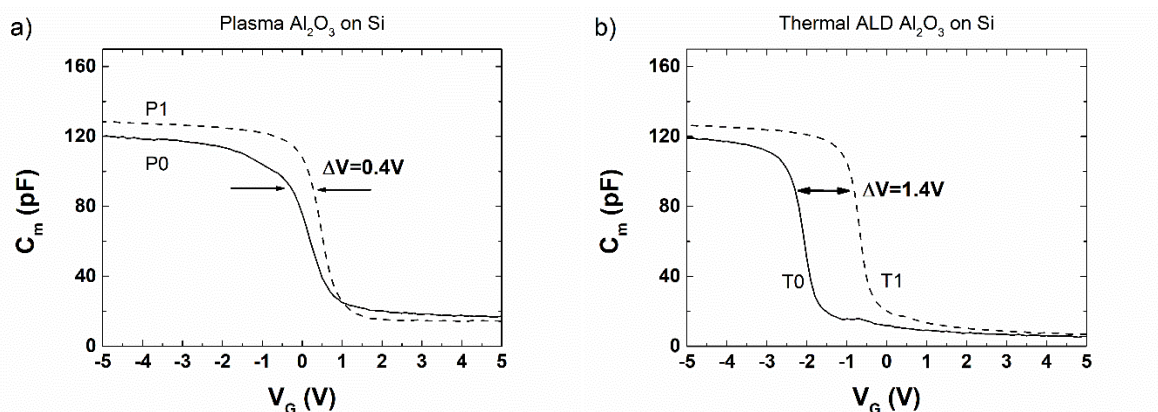


Figure 1: C-V scan at 1 MHz for as-deposited (solid lines) and annealed (dashed lines) plasma ALD samples (a) and thermal ALD samples (b).

The C-V curves (Figure 1) of both plasma ALD (P0) and thermal ALD (T0) as-deposited samples are shifted towards more positive  $V_G$  values after annealing (P1, T1 respectively), which indicates the activation of negative charges. As expected, the shift of the capacitance curve is larger for thermal ALD since negative charges are already present in as-deposited plasma ALD sample (P0) and the impact of annealing on the field-effect passivation is moderate [30].

The flat band voltage ( $V_{FB}$ ) was calculated, in order to evaluate the fixed oxide charges  $Q_{ox}$  by [6], [29]:

$$Q_{ox} = (\varphi_{ms} - V_{FB}) C_{ox} \quad (3)$$

where  $\varphi_{ms}$  is the work function difference between the metal gate and the semiconductor; it was calculated to be -0.94 V (for Al gate and p-doped Si with  $2 \times 10^{16} \text{ cm}^{-3}$  dopant concentration which corresponds to our samples resistivity of  $0.8 \text{ } \Omega\text{cm}$  [31]). In order to extract  $V_{FB}$ ,  $1/C_m^2$  was plotted [6]; the total capacitance in the depletion regime varies linearly with  $V_G$ :

$$\frac{1}{C_m^2} = \frac{1}{C_{ox}^2} + \frac{2}{S^2 N_A q \epsilon_{Si}} (V_G - V_{FB}) \quad (4)$$

where  $N_A$  is the acceptor doping level,  $q$  is the elementary charge,  $\epsilon_{Si} = 11.7 \epsilon_0$  is the dielectric permittivity of silicon and  $S$  is the surface area of the capacitor. Using eq. 4 we found  $V_{FB}$  by extrapolation, and subsequently calculated  $Q_{ox}$  from eq. 3 (values for all 4 samples are shown in Table II). Although charges are always reported to be negative in annealed T-ALD or P-ALD  $\text{Al}_2\text{O}_3$  samples, positive charges have also been reported for as-deposited T-ALD  $\text{Al}_2\text{O}_3$  samples [32], [33].  $Q_{ox}$  was then used to estimate the electric field in the space charge region of Si from the Gauss equation (Table II):

$$E_{dc} = \frac{Q_{ox}}{\epsilon_{Si}} \quad (5)$$

For the interface trap density  $D_{it}$  extraction, we used the high-low frequency C-V technique [6] where the measurements were taken at two different frequencies (1 MHz and 10 kHz). Figure 2 shows  $D_{it}$  versus the gate voltage for the plasma samples, both as-deposited (a) and after annealing (b). The high-low frequency extraction method gives  $D_{it}$  in the voltage range spanning from flat band to weak inversion [6]. For process monitoring, as is in our case, a single  $D_{it}$  value determined at a specific point on the C-V curve in this voltage range is sufficient [6]. We identified the  $D_{it}$  value corresponding to  $V_G = V_{FB} + 5\% V_{FB}$  for each sample. The results are shown in Table II. For the thermal ALD samples (curves not shown here), the  $D_{it}$  responding to 10 kHz were below the measurement sensitivity ( $10^{10} \text{ cm}^{-2} \text{ eV}^{-1}$ ). Smaller values of  $D_{it}$  for the T0-T1 samples are expected, because of the higher hydrogen concentration due to the  $\text{H}_2\text{O}$  oxidant in the thermal ALD process [34]. Additionally, the high

$D_{it}$  value for the annealed plasma sample is consistent with its very low minority carrier lifetime.

The  $D_{it}$  concentration decreases after annealing for both processes because of the diffusion of H atoms present in the dielectric layer towards the dielectric/Si interface [23]. All these electrical parameters extracted from C-V curves and shown in Table II, will be used for the SHG data interpretation.

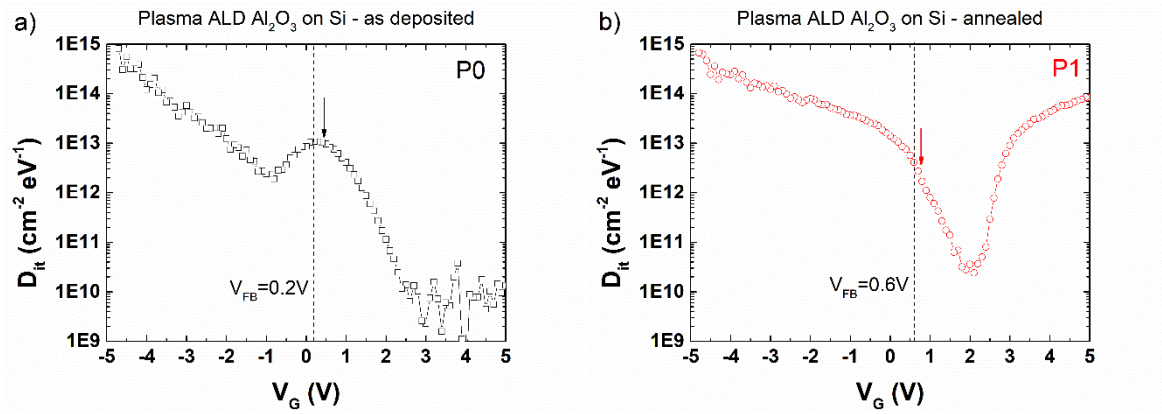


Figure 2:  $D_{it}$  vs  $V_G$  for plasma ALD samples. Approximate values of  $D_{it}$  are indicated by arrows in the depletion region.

Table II: C-V characterization results for Si samples passivated with a 15 nm  $Al_2O_3$  film

Sample	$V_{FB}$ (V)	$Q_{ox}$ ( $\times 10^{12} \text{ cm}^{-2}$ )	$E_{dc}$ ( $\times 10^5 \text{ V/cm}$ )	$D_{it}$ ( $\text{eV}^{-1} \text{ cm}^{-2}$ )
P0	0.2	-2.64	+4.04	$10^{13}$
P1	0.6	-3.58	+5.48	$3 \times 10^{12}$
T0	-2	+2.85	-4.36	$< 10^{10}$
T1	-0.6	-0.5	+0.77	$< 10^{10}$

The lifetime and C-V measurements are consistent. Reducing the surface trap density ( $D_{it}$ ) to values lower than  $10^{11} \text{ eV}^{-1} \text{ cm}^{-2}$  is compulsory to improve the passivation and consequently increase lifetime. Indeed low lifetime values (samples P0, P1) are associated to high values of  $D_{it}$ , while T-ALD samples (T0, T1) with very low  $D_{it}$  have a high  $\tau_{eff}$ . Moreover, higher lifetime is obtained after annealing (Table I) thanks to field effect passivation which is also reflected in the increase of  $Q_{ox}$  (Table II).

### III. SHG characterization

#### A. Measurement setup

The SHG measurements were performed using the Harmonic F1X<sup>®</sup> wafer inspection system developed by Femtometrix [35]. A pump laser operating at 780 nm irradiates the sample with pulses of 90 fs duration, 80 MHz repetition rate and an average power of 364 mW. The laser beam passes through a half wave plate which controls the angle of the linear polarization with respect to the plane of incidence and subsequently is focused on the sample surface with a minimum spot size of approximately 50 $\mu$ m for a 45 $^\circ$  angle of incidence. Generated SH radiation passes through a collimator and a set of filters which separate it from the reflected fundamental light. The SH beam is then detected along a specific polarization direction and enters a photomultiplier tube and a gated photon counter. In this work the incident fundamental and the SH radiations were both polarized parallel (P) to the plane of incidence while the angle of incidence was set at 45 $^\circ$ , unless otherwise stated.

#### B. Time-dependent SHG

Figure 3 shows the time-dependent SHG (TD-SHG) signal from the samples, recorded for 1000 seconds. SHG variation in time is attributed to the EFISH effect [12]–[15]. Plasma ALD samples (P0, P1) exhibit both higher initial ( $t=0$ ) and saturation ( $t=1000$ s) SHG values than thermal ALD samples (T0, T1). The first data point on each curve can be associated with the interface structural properties and its static electric field ( $\chi^{(2)}$  and  $E_{dc}$  correspondingly in eq. 2). Therefore, this first point probes the initial fixed charges and potentially some charged interface traps before any significant laser-induced charge-trapping occurs (Figure 3b). As the laser keeps illuminating the sample (Figure 3c), two main competing phenomena give rise to time-dependent EFISH ( $E(t)$  in eq. 2):

- The fundamental beam creates electron-hole pairs in Si which can be separated by the pre-existing interface dc field. In the case of Al<sub>2</sub>O<sub>3</sub> with negative charges this would decrease the SHG intensity, which is not the case in Figure 3a.
- The electrons from the Si valence band can be injected into the conduction band of Al<sub>2</sub>O<sub>3</sub> and get trapped in interface or bulk states in the oxide. This happens when the electrons overcome the energy barrier at the oxide/Si interface by 2- or 3- photon absorption processes or alternatively through tunneling [21], therefore increasing the initial electric field. After the trap sites are filled, SHG reaches saturation.

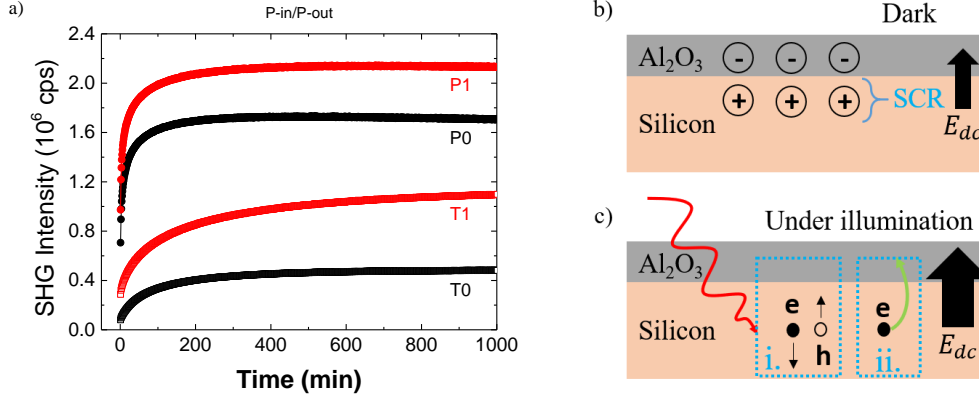


Figure 3: (a) Time-dependent SHG measurements on 15 nm ALD thermal and plasma  $\text{Al}_2\text{O}_3$  on Si (100) samples (as-deposited in black and annealed in red). b) Static electric field at the interface caused by negative fixed charges in  $\text{Al}_2\text{O}_3$  under dark conditions. The negative charges induce positive charges in the Si space charge region. c) Under illumination the electric field is modified: i) electron-hole pairs are created in Si and are separated by the pre-existing field, ii) electrons from the Si valence band can be injected into the oxide via a multi-photon process.

Therefore, the TD-SHG gives information on the charge trapping kinetics. In the case of  $\text{Al}_2\text{O}_3$  on Si, charging occurs from photo-generated electrons inside the silicon substrate which are injected at the interface or inside the bulk of the oxide [16]. In our case, injection of charges at the  $\text{Al}_2\text{O}_3$ /air interface is unlikely to occur since the thickness of the  $\text{Al}_2\text{O}_3$  film is 15 nm. It must be also noted that when depositing  $\text{Al}_2\text{O}_3$  on Si, even on a H-terminated surface (after HF etch), there is always an interfacial  $\text{SiO}_x$  layer [38] in the 0.1-1 nm range which might play a role in charge transfer. Generally, the TD-SHG in  $\text{SiO}_2$ /Si stacks can be fitted by one or more exponentials which are typically associated with one or more charging mechanisms attributed to different kinds of traps [13], [36]. In  $\text{Al}_2\text{O}_3$  oxide, the O interstitial ( $\text{O}_i$ ) and Al vacancy ( $\text{V}_{\text{Al}}$ ) point defects have an energy below mid-gap in the  $\text{Al}_2\text{O}_3$  bandgap and can be negatively charged [37].

In order to compare the time dependencies between our samples, the experimental data were fitted by two exponentials:

$$\sqrt{I_{2\omega}(t)} \propto a_0 + a_1(1 - e^{-t/\tau_1}) + a_2(1 - e^{-t/\tau_2}) \quad (6)$$

where  $a_i$  are constants and  $\tau_i$  are the time constants associated to charging mechanisms. This simple equation is sufficient to reproduce the experimental curves. In all cases an initial fast signal increase is followed by a slower time variation. The fitting curves for all samples are shown in Figure 4 and the fitting parameters are reported in Table III.

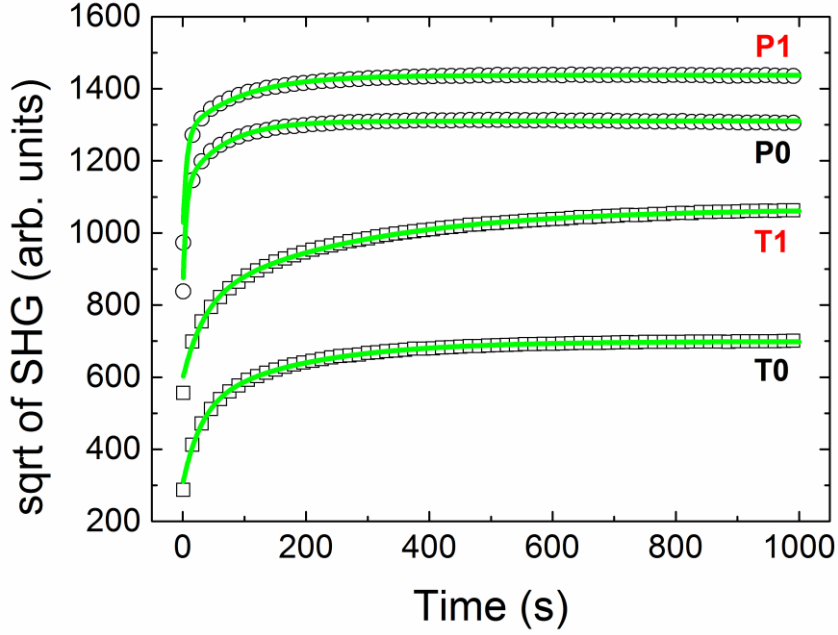


Figure 4: Square root of the SHG signal versus time and fitting curves (green solid lines) with two exponentials for all samples. For visual clarity, the number of data points represented was reduced.

Comparing the two processes, we see that T0-T1 samples have higher time constants than P0-P1 samples, indicating faster trapping for plasma ALD samples, which is consistent with the larger values of  $D_{it}$  measured by C-V. Generally, the higher  $D_{it}$  concentrations are associated with the smaller time constants. Annealing the as-deposited samples (P0, T0) caused an increase in both time constants. The larger time constants  $\tau_2$ , connected with the slow increase of SHG, can be associated to the saturation of trapping sites [21]. The fact that annealing passivates the interface traps (verified by the noticeable decrease of the  $D_{it}$  values in Table III) can explain the increase in both time constants.

Table III: TD-SHG fitting results for Si samples passivated with a 15 nm  $Al_2O_3$  film

Sample	$D_{it}$ ( $eV^{-1} cm^{-2}$ )	$\tau_1$ (s)	$\tau_2$ (s)
P0	$10^{13}$	5	63
P1	$3 \times 10^{12}$	6	90
T0	$< 10^{10}$	29	172
T1	$< 10^{10}$	35	268

### C. Initial SHG (at t=0)

In this section we focus on the initial SHG values at t=0 which we correlate with the minority carrier lifetime  $\tau_{\text{eff}}$  extracted from  $\mu$ -PCD and with the  $E_{\text{dc}}$  values calculated from C-V curves. We observe higher initial SHG for the plasma ALD (P0, P1) than for the thermal ALD (T0, T1) process, which can be accredited to the higher  $Q_{\text{ox}}$  density and the higher initially charged  $D_{\text{it}}$  in the former. Furthermore, for each process separately, the SHG intensity increases after annealing, which is consistent with the increase of fixed negative charge  $Q_{\text{ox}}$ , causing the enhancement of  $E_{\text{dc}}$ . Figure 5 compares the normalized initial SHG values (at t=0) with the normalized lifetime values (from Table I). It is clear that both carrier lifetime and SHG increase after annealing. Minority carrier lifetime is theoretically proportional to  $Q_{\text{ox}}^2/D_{\text{it}}$  [4], [38], and SHG is proportional to  $Q_{\text{ox}}^2$ , since the SHG signal depends quadratically on  $E_{\text{dc}}$  (eq. 2 and eq.5). Note that the SHG may vary when scanned across a sample, depending on the local properties (electric field, thickness, etc...). The initial SHG was measured on 300 points across each sample and the mean value as well as the standard deviation were calculated (Table IV). The high standard deviation for the T1 sample is consistent with the high  $\tau_{\text{eff}}$  dispersion observed on this sample (results not shown here).

Table IV: Mean value and standard deviation for initial SHG, calculated from maps on each sample.

Sample	Mean initial SHG ( $10^5$ cps)	Std. deviation
P0	6.74	1.7%
P1	9.53	2.5%
T0	0.83	2.5%
T1	2.74	12.5%

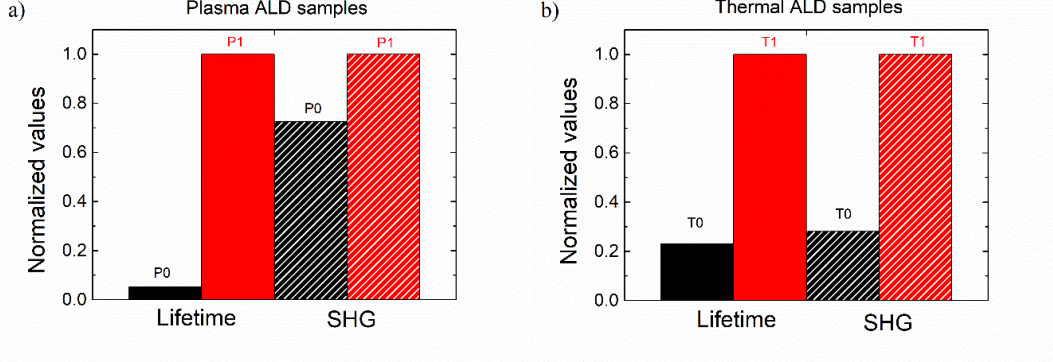


Figure 5: Normalized carrier lifetimes measured by  $\mu$ -PCD and normalized SHG signals for as-deposited and annealed samples prepared with plasma (a) and thermal (b) ALD processes. The normalization was done for each set with the respective maximum of each measurement technique.

Rewriting eq. 2 at  $t=0$ , the square root of the SH intensity is roughly proportional to  $E_{dc}$ :

$$\sqrt{I_{2\omega}} \propto |\chi^{(2)} + \chi^{(3)} E_{dc}| I_{\omega} \quad (7)$$

In order to associate the initial SHG signal with the static electric field  $E_{dc}$  induced by pre-existing  $Q_{ox}$  and charged  $D_{it}$ , the square root of the initial SHG for each sample is plotted versus  $E_{dc}$ , calculated from the C-V curves (see Figure 6). The linear relationship between  $\sqrt{I_{2\omega}}$  and  $E_{dc}$  (eq. 7) agrees fairly well with the SHG experimental data. Therefore, SHG is well suited to probe the oxide/Si interface electric field and EFISH is the main contribution to the initial second harmonic signal in our samples.

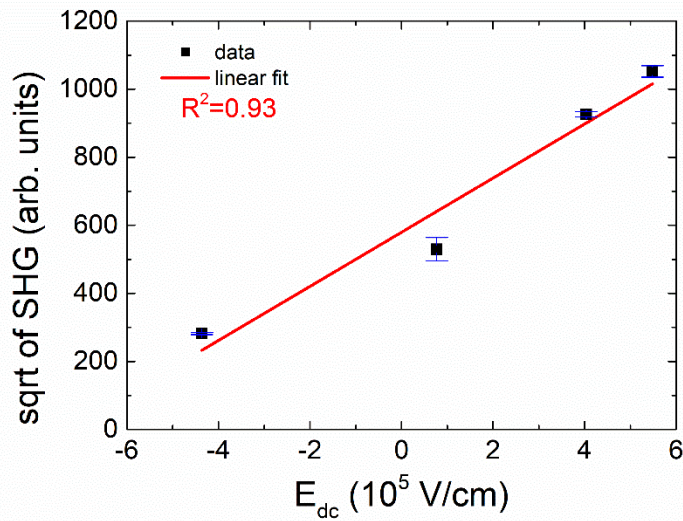


Figure 6: Square root of the initial SHG signal versus the static electric field calculated from C-V measurements on MOS capacitors. Error bars were calculated from the standard deviation in Table IV, accounting for propagation of error when converting to the square root of SHG.

## IV. Simulation

### A. Simulator description

The SHG signal originating from thin film layered structures is influenced by the optical effects. The fundamental  $I_\omega$ , as well as the SHG radiation  $I_{2\omega}$ , propagate inside the structures, are absorbed, reflected and transmitted at the different interfaces between adjacent media, and potentially exhibit interferences due to multiple reflections in the stratified thin films [39]. Therefore, when comparing structures with different film thicknesses or when varying the angle of incidence in SHG experiments, the optical path is modified and these effects will influence the measurements. In order to access electrical parameters, one must anticipate the impact of optical effects on SHG by using proper simulation.

Figure 7a shows the  $\text{Al}_2\text{O}_3/\text{Si}$  structure under study. Our in-house simulation tool uses a matrix formalism [40] in order to estimate the optical electric field at the fundamental and SH frequency at the positions highlighted with circles in Figures 7b and 7c. All of the fields are P-polarized (lying in the x-z plane). The incident field amplitude is denoted by  $E_{1-}^\omega$ , the reflected one by  $E_{1+}^\omega$  and the total transmitted one by  $E_{3-}^\omega$ . The fundamental electric field at the interface between  $\text{Al}_2\text{O}_3$  and Si generates the SH nonlinear polarization  $P_i^{NL}(2\omega)$ . The reflected SH wave is denoted by  $E_{1+}^{2\omega}$  and the totally transmitted one by  $E_{3-}^{2\omega}$ . It should be mentioned that the physical boundary condition of no incident light at  $2\omega$  is imposed,  $E_{1-}^{2\omega} = 0$ . Additionally, no incoming light from the bottom of the substrate ( $E_{3+}^\omega = 0, E_{3+}^{2\omega} = 0$ ) towards the oxide is considered, since the penetration depth of the fundamental beam at 780 nm in silicon is  $10\mu\text{m}$  while that of the SH beam is only 67 nm [41].

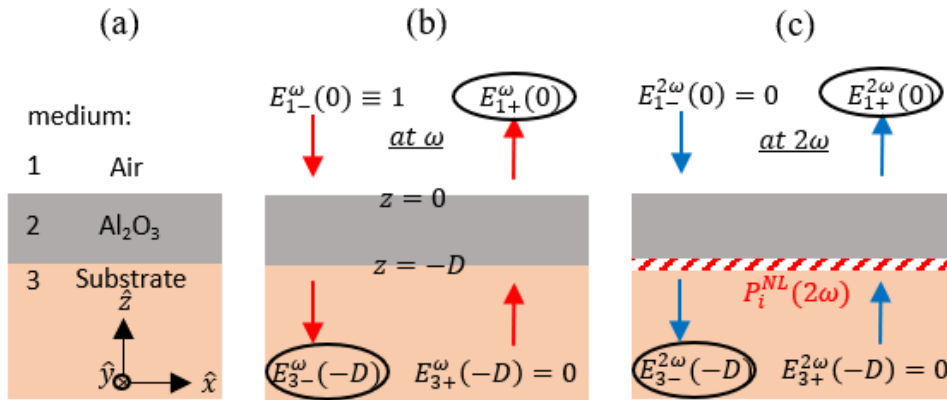


Figure 7: a) Sample geometry. Boundary conditions and calculated fields (circled) for: b) the fundamental frequency and c) the SH frequency. The nonlinear polarization at the interface is also shown in (c).

For the calculation of the SH radiation, the nonlinear polarization created by the fundamental field is added as a source term in Maxwell's equations at each interface. With a p-polarized incident and SHG wave, the 2<sup>nd</sup> order polarization at an interface between a dielectric and Si(100) is given by[42]:

$$P_{2\omega}^{Pp} \propto \left[ \chi_{zzz}^{(2)} F_s f_s^2 + \chi_{zxx}^{(2)} F_s f_c^2 - \chi_{zxx}^{(2)} 2F_c f_s f_c - \frac{i}{4} n_\omega \zeta (3F_c f_c^2 f_s + 4F_s f_s^2 f_c + F_c f_s f_c) \right] E_\omega^2 \quad (8)$$

where  $f_s$ ,  $f_c$ ,  $F_s$ ,  $F_c$  are the Fresnel factors:  $f_s = \sin\theta / n_\omega$ ,  $f_c = \cos\theta / n_\omega$ ,  $F_s = \sin\theta / n_{2\omega}$ ,  $F_c = \cos\theta / n_{2\omega}$ ;  $\chi_{ijk}^{(2)}$  are the 2<sup>nd</sup> order interface susceptibility tensor elements;  $n_\omega$  is the refractive index of Si;  $\zeta$  is the bulk quadrupolar susceptibility;  $E_\omega$  is the fundamental electric field.

In order to accommodate the extra interfacial electric field term in the previous expression,  $E_{dc}$  is added phenomenologically to the  $\chi_{zzz}^{(2)}$  component, which is the prominent interface susceptibility term in eq.8, giving rise to a 2<sup>nd</sup> order polarization in the vertical z-direction parallel to the dc field. The new expression becomes:

$$P_{2\omega}^{Pp} \propto \left[ \left( \chi_{zzz}^{(2)} + \chi^{(3)} E_{dc} \right) F_s f_s^2 + \chi_{zxx}^{(2)} F_s f_c^2 - \chi_{zxx}^{(2)} 2F_c f_s f_c - \frac{i}{4} n_\omega \zeta (3F_c f_c^2 f_s + 4F_s f_s^2 f_c + F_c f_s f_c) \right] E_\omega^2 \quad (9)$$

This non-linear polarization is used as source term in Maxwell equations and the locally generated second harmonic field ( $E_{2\omega}$ ) is calculated from the boundary conditions at each interface. The second harmonic field generated at the interface is then propagated throughout the structure and the SH intensity coming out the sample is calculated from the squared modulus of the SH field in air ( $E_{1+}^{2\omega}(0)$  in Figure 7c).

The simulation parameters that can be modified are: the wavelength of the incident radiation, the angle of incidence, the fundamental and SH polarizations, the number of layers, the thickness and the complex refractive indices (including absorption) of each layer, as well as the  $E_{dc}$  field.

## B. Simulation results

SHG was measured on three  $Al_2O_3/Si$  samples with different oxide thicknesses of 5, 15 and 25 nm before and after annealing (Figure 8), prepared with the thermal ALD procedure described in Section II.A. Note that both experimental and simulated SHG are

normalized, since an absolute-value comparison between the output of the photon-counter and the simulated optical power is not possible. The optical simulation reproduces the experimental thickness dependence trend of the SHG signal. It should be noted that no  $E_{dc}$  field was used for the simulation of the as-deposited samples, while an  $E_{dc}$  field of  $10^5$  V/cm was included into eq. 9 for the simulation of the annealed samples. Although this value might differ from one sample to another (which could explain the difference between the experimental data and the fit), it has been shown [4] that after annealing, the fixed charge density located close to the  $\text{Al}_2\text{O}_3/\text{Si}$  interface reaches a maximum value for an  $\text{Al}_2\text{O}_3$  thickness around 5 nm and remains constant for thicker films. In any case, both propagation related phenomena (that are modified with the film thickness) and interface electric field must be considered when analyzing the SHG response.

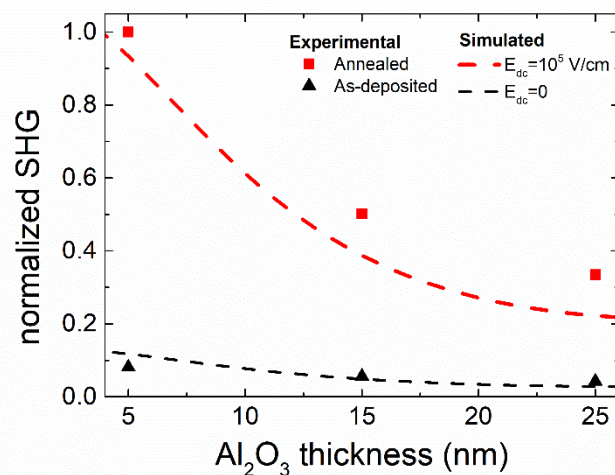


Figure 8: Experimental and simulated SHG intensity versus  $\text{Al}_2\text{O}_3$  thickness. The measurements and simulations were performed at  $45^\circ$  incidence angle.

An approach of finding  $E_{dc}$  for both as-deposited and annealed samples with the same film thickness is to measure the SHG intensity versus the angle of incidence (AOI) since it alters the propagating path of the fundamental and harmonic beams, which inevitably affect the interference pattern. In Figure 9, the initial SHG signal (at  $t=0$ ) is monitored versus the angle of incidence of the fundamental radiation (data points). An offset is observed between the as-deposited and annealed samples for each ALD process. We attribute this difference to the change in  $E_{dc}$  after annealing. In order to investigate this, we simulate the SHG response before and after annealing using the values of  $E_{dc}$  calculated from C-V measurements (Table II).

The input parameters for the simulation, apart from the ones mentioned in the previous section and the  $E_{dc}$ , are the nonlinear susceptibility components in eq. 8 and eq. 9. The following values were used:  $\chi_{zz}^{(2)} = 5.8 \times 10^{-18} mV^{-1}$ ,  $\chi_{xzx}^{(2)} = 1.2 \times 10^{-18} mV^{-1}$ ,  $\chi_{zxx}^{(2)} = 0.043 \times 10^{-18} mV^{-1}$ ,  $\zeta = 4.4 \times 10^{-18} mV^{-1}$  [43] and for  $\chi^{(3)} \propto 10^{-24} m^2V^{-2}$  [10];  $\chi^{(3)}$  multiplied by  $E_{dc}$  (approximately  $10^5$  V/cm) has the same order of magnitude as the 2<sup>nd</sup> order components. However, the  $\chi^{(2)}$  values depend on the material preparation and process, and other values have been reported as well [44]. Furthermore, the sign and value of the  $E_{dc}$  term can cancel out the  $\chi_{zz}^{(2)}$  term in eq. 9. Therefore, since absolute values of  $\chi^{(2)}$  and  $\chi^{(3)}$  are difficult to obtain and depend on material preparation, we used a “differential” approach for simulating the AOI experiments:

1. We considered the as-deposited sample as a reference, which we simulated using only eq. 8 and the  $\chi^{(2)}$  values given above (in the previous paragraph).
2. We calculated the algebraic difference between the dc field magnitudes of as-deposited and annealed samples  $\Delta E_{dc}$  from Table II and we added it in the simulation using eq. 9. This curve was considered to correspond to the annealed sample.
3. Finally, a normalization was done by dividing each set (experimental and simulated) with its corresponding maximum value.

As seen in Figure 9, the optical simulation (solid lines) of SHG versus the angle of incidence agrees well with the actual experiment (symbols). This illustrates the potential of the simulation which includes optical phenomena to investigate indirectly the electrical properties or passivation quality ( $E_{dc}$  and thus  $Q_{ox}$ ) through contactless SHG experiments.

In order to extract real values of  $E_{dc}$  from stand-alone SHG measurements, one would have to calibrate the SHG model using various and numerous samples.

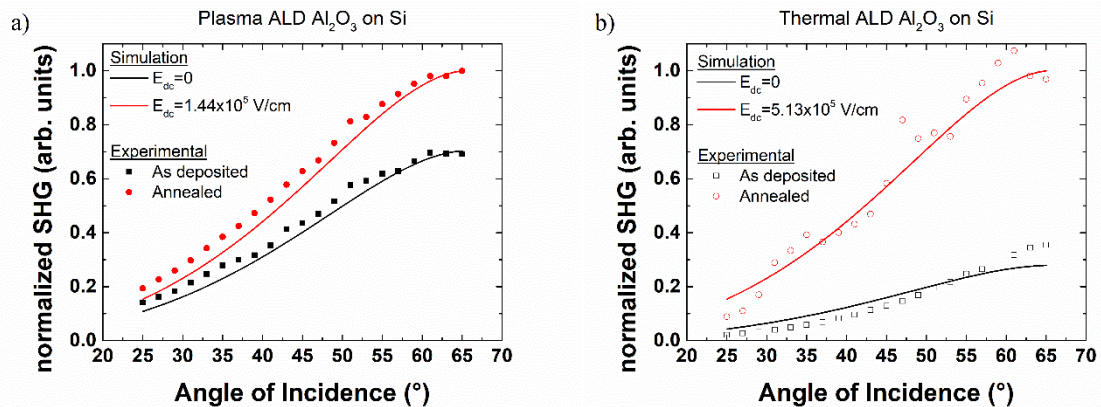


Figure 9: Normalized SHG intensity vs angle of incidence for plasma (a) and thermal (b) ALD  $\text{Al}_2\text{O}_3$ . The symbols are the experimental data for as deposited (black squares) and annealed (red circles) samples respectively. The black and red lines are the simulated data for an electric field variation at the interface which was calculated from the C-V curves. For the simulation, the as-deposited sample was treated as reference with  $E_{dc}=0$ , while for the annealed sample the value of  $E_{dc}$  was the difference between the electric fields of as-deposited and annealed samples. The normalization is done by dividing each set (experimental and simulated) with its corresponding maximum value. The fluctuations of the experimental data for the annealed thermal ALD sample are coherent with the high standard deviation of this sample (see Table IV).

## V. Conclusion

This paper investigated the capacity of SHG to monitor the field effect passivation due to oxide charges. The time-dependent dynamics of EFISH showed that the initial SHG signal is related mostly to the fixed  $Q_{ox}$  and the SHG time evolution is fast (slow) for high (low)  $D_{it}$  values. SHG measurements were correlated with minority carrier lifetime values corroborating the possibility for contactless SHG probing of  $\text{Al}_2\text{O}_3/\text{Si}$  interfacial quality. The conventional C-V measurements revealed the fixed charge density inside the oxide and helped estimating the static electric field at the interface. We showed that the square root of the SHG intensity scales linearly with the electric field value extracted from C-V, as expected theoretically. Finally, the optical interferences related to the thicknesses of the thin film structures were studied with our home-made simulator. SHG simulations which use the values of  $\Delta E_{dc}$  could reproduce the angle of incidence data. This confirms that by decorrelating optical phenomena, the combination of experiment and simulation paves the way for a pragmatic oxide charge quantitative analysis via SHG.

The SHG technique could be applied to most dielectric/semiconductor stacks (for example  $\text{SiO}_2/\text{Si}$ ,  $\text{SiN}_x/\text{Si}$ ,  $\text{Ta}_2\text{O}_5/\text{Si}$ ,  $\text{HfO}_2/\text{Si}$ , etc...). However, the following aspects must be considered:

- If the materials are non-centrosymmetric, they generate SH from their bulk, which can be orders of magnitude stronger than the SH induced at the interface.
- Optical parameters of the materials can modify the SHG response. For example, for highly absorbing materials/films the SH signal generated at the interface can be dramatically attenuated.

## Acknowledgments

Authors thank Region Rhône Alpes (ARC6 program) for funding.

## References

- [1] G. J. Gerardi, E. H. Poindexter, P. J. Caplan, and N. M. Johnson, "Interface traps and Pb centers in oxidized (100) silicon wafers," *Appl. Phys. Lett.*, vol. 49, pp. 348–350, 1986.
- [2] C. R. Helms and E. H. Poindexter, "The silicon-silicon-dioxide system: its microstructure and imperfections," *Rep. Prog. Phys.*, vol. 57, pp. 791–852, 1994.
- [3] G. Dingemans, R. Seguin, P. Engelhart, M. C. M. van den Sanden, and W. M. M. Kessels, "Silicon Surface Passivation by ultrathin Al<sub>2</sub>O<sub>3</sub> films synthesized by thermal and plasma atomic layer deposition," *Phys. Status Solidi*, vol. 1–2, no. 1, pp. 10–12, 2010.
- [4] G. Dingemans and W. M. M. Kessels, "Status and prospects of Al<sub>2</sub>O<sub>3</sub>-based surface passivation schemes for silicon solar cells," *J. Vac. Sci. Technol. A*, vol. 30, p. 040802, 2012.
- [5] "ITRS," 2013. [Online]. Available: <http://www.itrs2.net/2013-itrs.html>.
- [6] Dieter K Schroder, *Semiconductor Material and Device Characterization*, 3rd ed. Wiley & Sons, 2006.
- [7] D. K. Schroder, "Carrier lifetimes in silicon," *IEEE Trans. Electron Devices*, vol. 44, no. 1, pp. 160–170, 1997.
- [8] M. Wilson, J. Lagowski, L. Jastrzebski, A. Savtchouk, and V. Faifer, "COCOS (corona oxide characterization of semiconductor) non-contact metrology for gate dielectrics," *AIP Conf. Proc.*, vol. 550, p. 220, 2001.
- [9] G. Lüpke, "Characterization of semiconductor interfaces by second-harmonic generation," *Surf. Sci. Rep.*, vol. 35, no. 3, pp. 75–161, 1999.
- [10] R. W. Boyd, *Nonlinear Optics*, 3rd ed. Academic Press, 2008.
- [11] T. F. Heinz, "Second-Order Nonlinear Optical Effects at Surfaces and Interfaces," *Nonlinear Surface Electromagnetic Phenomena*. pp. 353–416, 1991.
- [12] O. A. Aktsipetrov, A. A. Fedyanin, V. N. Golovkina, and T. V. Murzina, "Optical second-harmonic generation induced by a dc electric field at the Si–SiO<sub>2</sub> interface," *Opt. Lett.*, vol. 19, no. 18, p. 1450, Sep. 1994.
- [13] J. G. Mihaychuk, J. Bloch, Y. Liu, and H. M. Van Driel, "Time-dependent second-harmonic generation from the Si – SiO<sub>2</sub> interface induced by charge transfer," *Opt. Lett.*, vol. 20, no. 20, pp. 2063–2065, 1995.
- [14] J. G. Mihaychuk, N. Shamir, and H. M. Van Driel, "Multiphoton photoemission and electric-field-induced optical second-harmonic generation as probes of charge transfer across the Si/SiO<sub>2</sub> interface,"

- Phys. Rev. B*, vol. 59, no. 3, pp. 2164–2173, 1999.
- [15] J. Bloch, J. Mihaychuk, and H. van Driel, “Electron Photoinjection from Silicon to Ultrathin SiO<sub>2</sub> Films via Ambient Oxygen,” *Phys. Rev. Lett.*, vol. 77, no. 5, pp. 920–923, 1996.
- [16] V. Fomenko, E. P. Gusev, and E. Borguet, “Optical second harmonic generation studies of ultrathin high-k dielectric stacks,” *J. Appl. Phys.*, vol. 97, no. 8, pp. 1–8, 2005.
- [17] J. Price, M. Lei, P. S. Lysaght, G. Bersuker, and M. C. Downer, “Charge trapping defects in Si/SiO<sub>2</sub>/Hf (1–x)SixO<sub>2</sub> film stacks characterized by spectroscopic second-harmonic generation,” *J. Vac. Sci. Technol. B Microelectron. Nanom. Struct.*, vol. 29, p. 04D101, 2011.
- [18] J. J. H. Gielis, B. Hoex, M. C. M. Van De Sanden, and W. M. M. Kessels, “Negative charge and charging dynamics in Al<sub>2</sub>O<sub>3</sub> films on Si characterized by second-harmonic generation,” *J. Appl. Phys.*, vol. 104, p. 073701, 2008.
- [19] N. M. Terlinden, G. Dingemans, M. C. M. Van De Sanden, and W. M. M. Kessels, “Role of field-effect on c-Si surface passivation by ultrathin (2–20 nm) atomic layer deposited Al<sub>2</sub>O<sub>3</sub>,” *Appl. Phys. Lett.*, vol. 96, no. 11, pp. 2008–2011, 2010.
- [20] G. Dingemans, N. M. Terlinden, M. a. Verheijen, M. C. M. Van De Sanden, and W. M. M. Kessels, “Controlling the fixed charge and passivation properties of Si(100)/Al<sub>2</sub>O<sub>3</sub> interfaces using ultrathin SiO<sub>2</sub> interlayers synthesized by atomic layer deposition,” *J. Appl. Phys.*, vol. 110, no. 9, p. 093715, 2011.
- [21] N. M. Terlinden, G. Dingemans, V. Vandalon, R. H. E. C. Bosch, and W. M. M. Kessels, “Influence of the SiO<sub>2</sub> interlayer thickness on the density and polarity of charges in Si/SiO<sub>2</sub>/Al<sub>2</sub>O<sub>3</sub> stacks as studied by optical second-harmonic generation,” *J. Appl. Phys.*, vol. 115, no. 3, 2014.
- [22] G. Dingemans, N. M. Terlinden, D. Pierreux, H. B. Profijt, M. C. M. Van De Sanden, and W. M. M. Kessels, “Influence of the Oxidant on the Chemical and Field-Effect Passivation of Si by ALD Al<sub>2</sub>O<sub>3</sub>,” *Electrochem. Solid-State Lett.*, vol. 14, no. 1, pp. H1–H4, 2011.
- [23] G. Dingemans, F. Einsele, W. Beyer, M. C. M. Van de Sanden, and W. M. M. Kessels, “Influence of annealing and Al<sub>2</sub>O<sub>3</sub> properties on the hydrogen-induced passivation of the Si/SiO<sub>2</sub> interface,” *J. Appl. Phys.*, vol. 111, no. 9, p. 93713, 2012.
- [24] A. Stesmans and V. V Afanas’ev, “Si dangling-bond-type defects at the interface of (100)Si with ultrathin layers of SiO<sub>x</sub>, Al<sub>2</sub>O<sub>3</sub>, and ZrO<sub>2</sub>,” *Appl. Phys. Lett.*, vol. 80, no. 11, pp. 1957–1959, 2002.
- [25] K. B. Jinesh, J. L. Van Hemmen, M. C. M. Van De Sanden, F. Roozeboom, J. H. Klootwijk, W. F. A.

- Besling, and W. M. M. Kessels, "Dielectric Properties of Thermal and Plasma-Assisted Atomic Layer Deposited Al<sub>2</sub>O<sub>3</sub> Thin Films," *J. Electrochem. Soc.*, vol. 158, no. 2, pp. G21–G26, 2011.
- [26] "Semilab." [Online]. Available: [www.semilab.hu](http://www.semilab.hu).
- [27] F. Kersten, A. Schmid, S. Bordihn, J. W. Müller, and J. Heitmann, "Role of annealing conditions on surface passivation properties of ALD Al<sub>2</sub>O<sub>3</sub> films," *Energy Procedia*, vol. 38, no. 3494, pp. 843–848, 2013.
- [28] C. Barbos, D. Blanc-Pelissier, A. Fave, E. Blanquet, A. Crisci, E. Fourmond, D. Albertini, A. Sabac, K. Ayadi, P. Girard, and M. Lemiti, "Characterization of Al<sub>2</sub>O<sub>3</sub> thin films prepared by thermal ALD," *Energy Procedia*, vol. 77, pp. 558–564, 2015.
- [29] E. H. Nicollian and J. R. Brews, *MOS (Metal Oxide Semiconductor) Physics and Technology*. New York, USA: John Wiley & Sons, 1982.
- [30] J. Benick, A. Richter, T.-T. A. Li, N. E. Grant, K. R. McIntosh, Y. Ren, K. J. Weber, M. Hermle, and S. W. Glunz, "Effect of a post-deposition anneal on Al<sub>2</sub>O<sub>3</sub>/Si interface properties," in *2010 35th IEEE Photovoltaic Specialists Conference*, 2010, pp. 000891–000896.
- [31] W. M. Werner, "The work function difference of the MOS-system with aluminium field plates and polycrystalline silicon field plates," *Solid. State. Electron.*, vol. 17, pp. 769–775, 1974.
- [32] N. Batra, J. Gope, J. Panigrahi, R. Singh, and P. K. Singh, "Influence of deposition temperature of thermal ALD deposited Al<sub>2</sub>O<sub>3</sub> films on silicon surface passivation," *AIP Adv.*, vol. 5, p. 067113, 2015.
- [33] J. M. Rafi, M. Zabala, O. Beldarrain, and F. Campabadal, "Deposition Temperature and Thermal Annealing Effects on the Electrical Characteristics of Atomic Layer Deposited Al<sub>2</sub>O<sub>3</sub> Films on Silicon," *J. Electrochem. Soc.*, vol. 158, no. 5, p. G108, 2011.
- [34] G. Dingemans, W. Beyer, M. C. M. van de Sanden, and W. M. M. Kessels, "Hydrogen induced passivation of Si interfaces by Al<sub>2</sub>O<sub>3</sub> films and SiO<sub>2</sub>/Al<sub>2</sub>O<sub>3</sub> stacks," *Appl. Phys. Lett.*, vol. 97, no. 15, p. 152106, 2010.
- [35] "Femtometrix." [Online]. Available: [www.femtometrix.com](http://www.femtometrix.com).
- [36] T. Scheidt, E. G. Rohwer, H. M. von Bergmann, and H. Stafast, "Charge-carrier dynamics and trap generation in native Si/SiO<sub>2</sub> interfaces probed by optical second-harmonic generation," *Phys. Rev. B*, vol. 69, no. 16, p. 165314, Apr. 2004.
- [37] J. R. Weber, A. Janotti, and C. G. Van De Walle, "Native defects in Al<sub>2</sub>O<sub>3</sub> and their impact on III-V/Al<sub>2</sub>O<sub>3</sub> metal-oxide-semiconductor-based devices," *J. Appl. Phys.*, vol. 109, p. 033715, 2011.

- [38] B. Hoex, J. J. H. Gielis, M. C. M. Van De Sanden, and W. M. M. Kessels, "On the c-Si surface passivation mechanism by the negative-charge-dielectric Al<sub>2</sub>O<sub>3</sub>," *J. Appl. Phys.*, vol. 104, no. 11, 2008.
- [39] E. Hecht, *Optics*, 4th ed. Addison-Wesley, 2002.
- [40] O. S. Heavens, *Optical properties of thin solid films*. Courier Corporation, 1965.
- [41] M. A. Green, "Self-consistent optical parameters of intrinsic silicon at 300 K including temperature coefficients," *Sol. Energy Mater. Sol. Cells*, vol. 92, pp. 1305–1310, 2008.
- [42] J. E. Sipe, D. J. Moss, and H. M. Vandriel, "Phenomenological Theory of Optical 2nd-Harmonic and 3rd-Harmonic Generation from Cubic Centrosymmetric Crystals," *Phys. Rev. B*, vol. 35, no. 3, pp. 1129–1141, 1987.
- [43] Y. Q. An, R. Carriles, and M. C. Downer, "Absolute phase and amplitude of second-order nonlinear optical susceptibility components at Si(001) interfaces," *Phys. Rev. B*, vol. 75, no. 24, pp. 1–4, 2007.
- [44] M. Falasconi, L. C. Andreani, A. M. Malvezzi, M. Patrini, V. Mulloni, and L. Pavesi, "Bulk and surface contributions to second-order susceptibility in crystalline and porous silicon by second-harmonic generation," *Surf. Sci.*, vol. 481, no. 1–3, pp. 105–112, Jun. 2001.